POS-GRADUAÇÃO
DINÂMICA
DOS OCEANOS
E DA TERRA
UFF

ESTIMATION OF RETURN PERIODS OF WIND SPEED AND GUST AND SIGNIFICANT WAVE HEIGHT IN THE SOUTHWEST ATLANTIC

Emille Mazzaro Dias
emille.mazzaro@gmail.com
Rio de Janeiro Federal University - UFRJ, Rio de Janeiro, RJ, Brazil.

Ana Cristina Pinto de Almeida Palmeira
anactn@gmail.com
Rio de Janeiro Federal University - UFRJ, Rio de Janeiro, RJ, Brazil.

Renata Libonati
renata.libonati@igeo.ufrj.br
Rio de Janeiro Federal University - UFRJ, Rio de Janeiro, RJ, Brazil.

ABSTRACT

The Southwest Atlantic region hosts the two main oil basins in Brazil: Campos Basin and Santos Basin. In these regions, the study of extreme events and the estimation of return level are crucial issues to ensure the structural safety of ships, offshore platforms and coastal constructions. The knowledge of the wave and wind regime of a region is indispensable because from this analysis it is possible to estimate the energy load that a structure may be subjected to during its lifetime. In this context, the present work aims to estimate the 100-year return level of the variables: significant wave height (Hs), wind speed and gust at 10 m for each direction in the two main oil basins in Brazil. For this, data from ECMWF's ERA5 Reanalysis over the period 1979-2019 and the Peaks Over Threshold (POT) statistical model were used, using the Maximum Likelihood estimator. The results show that the SE, S and NW directions returned the highest return level values for wind speed. According to the analysis of the gusts results, the largest values were between 20 m/s and 30 m/s and considering the highest confidence interval, the values reached 38.64 m/s for the S direction. In the results of the return level estimates for Hs, it was found that the largest swells were from SW. With this, it is concluded that: although in situ observed data are preferable when conducting a study of extremes, reanalysis is a great alternative for limited locations of collected data. Another finding was that the POT Model is an excellent tool for the study of extremes, as it is improved and can select a more consistent and larger number of values than previously used models.

Keywords: Wind; Wave; Return period; Oil basins.

1. INTRODUCTION

According to the National Water Agency (ANA) the Southwest Atlantic Hydrographic Region occupies 2.5% of the national territory and covers five states: Minas Gerais, Espírito Santo, Rio de Janeiro, São Paulo and Paraná. According to the National Petroleum Agency (ANP), the Southwest Atlantic Ocean is home to the two main sedimentary areas already explored in the offshore oil and gas sector in the country, the Campos Basin (BC) and the Santos Basin (BS).

The BC extends from the vicinity of the city of Vitória - ES to Arraial do Cabo - RJ, being the second most important Basin in the country, concerning oil and gas production (PETROBRAS, 2020). It is considered a large open-air laboratory, for being a testing ground for the main offshore technologies, where it was possible to develop systems that later allowed the extraction of oil in deep and ultra-deep waters. BC, currently responsible for the largest oil and gas production, is the largest offshore sedimentary basin in the country (ANP, 2020). It has growth potential since it contains the pre-salt layer that has been explored since 2012 for being composed of large accumulations of light oil that has excellent quality and high commercial value (PETROBRAS, 2020). The extent of the Basin ranges from the southern coast of Rio de Janeiro to the northern part of the state of Santa Catarina.

Given the economic importance of the oil and gas industry for the country, the safety of offshore operations and the preservation of the environment must be taken into consideration. Thus, in recent years, the companies, through their various operational agencies and research centres, have developed procedures and technologies to mitigate damage caused by accidents in their operations, highlighting the importance of research that contributes to this end. Efforts to install meteoceanographic measurements have been made, but they are still insufficient, especially over the South Atlantic Ocean where the density of measurements is much lower compared to the Northern Hemisphere (Babanin et al., 2019), making research in this region difficult. The limitations in implementing equipment over the ocean include economic aspects (due to the high cost and difficulty in installation) as well as data collection (due to oceanic and atmospheric instabilities in their various phenomena) (Babanin et al., 2019). In situ collections are commonly related to fixed and drifting meteoceanographic buoys and are preferable due to the degree of reliability. However, remote forms of information collection should be considered. Satellites are an excellent alternative and can be applied to various parameters with the advantage of high spatial and temporal resolution. In countries like Brazil that do not have the constant availability of conventional meteoceanographic data, satellites become a viable and affordable option. Another way to estimate the environment in the oceanic regions is through numerical models and meteorological reanalysis datasets, which provide measurements of various parameters at regular intervals with long periods, usually decades. Among the reanalyses, some of the most widely used are ERA5 from the European Centre for Medium-Range Weather Forecasts (ECMWF) (Hersbach et al., 2019) and Climate Forecast System Reanalysis (CFSR) from the National Centers for Environmental Prediction (NCEP) in its second version (Saha et al., 2010).

An important variable studied, for any offshore activity, is wind. Wind over the ocean surface causes dynamic effects, such as inducing tangential drag stress related to wind speed. This stress applied to the surface is transmitted to the interior of the fluid by the effect of water viscosity and the turbulence of the flow, thus promoting a momentum transmission from the atmosphere to the ocean, enabling water movement (Phillips, 1986). The knowledge of the surface gravity waves generated by the wind is directly related to the safety of activities connected to the ocean, the development of these actions is based on 3 factors: wind intensity, duration and track, being the last one related to the extension of the space in which the wind remained constant in direction. They can be classified as swells, when they are still in the generation zone and/or are receiving energy from the wind, and swells when they have already propagated out of the generation zone and/or are not receiving energy from the wind (Pond and Pickard, 1983).

In the region of this study, high wave events are not as frequent when compared to the coast of South Africa and the North Atlantic (Candella and Souza, 2013). However, when they occur, they can lead to serious problems, because these waves, in most cases, are formed in distant locations (swells) and have great energy that propagates to the basins of the Brazilian coast (Mello Filho et al., 1993).

Highlighting the importance of studying the wind and wave regime for offshore and coastal structure construction projects, which requires knowledge of the severe conditions of the region, the study of extreme values is indispensable, because from the result it is possible to measure and project the energy load that a structure may be subjected during its lifetime. In this context, the present work aims to estimate the return levels of wind speed and gust at 10 m and Hs for a return period of 100 years in the Campos and Santos Basin regions. The analysis of extremes chosen is the Peaks Over Threshold (POT), belonging to the Generalized Pareto Distribution (GPD), currently considered one of the most consistent tools in the study of extremes because it can capture a larger number of possible values if compared to other distributions (Silva, 2013). For the use of the model, data from the ERA5 reanalysis were used.

2. DATA DESCRIPTION

Data

ERA5 ECMWF's ERA5 (Hersbach et al., 2019) reanalysis came to replace the former ERA-Interim (Dee et al., 2011) which has a spatial resolution of 79 km and temporal resolution of 6 hours. ERA5 is based on 4D-Var data assimilation using Integrated Forecasting System (IFS) Cycle 41r2. The change from ERA-Interim to ERA5 represents a gain in the overall quality of the reanalysis and in the level of detail, such as the spatial resolution, which now has 31 km grid spacing and 137 pressure levels, compared to ERA-Interim which has 79 km and 60 pressure levels.

For the development of this study, Wind data at 10 m (U and V wind components and wind gust at 10 m) and wave data (Hs) were used. The time series used consists of 41 years (1979-2019) of hourly and point data from the ERA5 reanalysis. For wind data, 5 locations were used, while 18 locations were used for Hs (Figure 1). Through Figure 1, points, where it was possible to calculate the return levels for all directions, are indicated in red, while the points in blue indicate not containing the minimum number of observations (at least one per year) in certain directions to perform the calculations. This is because NW winds usually appear quickly in a pre-frontal gyre situation, not contributing to the wind persistence that is needed to form mature waves relevant to the study.

The choice of the 5 points for the wind study was derived from a cluster analysis based on the same data for the study region, while for the Hs study a spacing of 1º latitude and longitude was used for the choice of the 18 points.

3. MATERIAL AND METHODS

Peaks Over Threshold (POT) Model

In this work, we used the Model of Excesses Above Threshold, more commonly known as Peaks Over Threshold - (POT), which is a statistical model from the 1980s to be employed in the area of hydrology. It became known through the works of Simiu and Heckert (1996), Abild et al., (1992), Hosking and Wallis (1987), where they presented a new distribution called Generalized Pareto Distribution (GPD). This was designed to specifically solve the tail estimation problem, in other words, to model excesses above a threshold.

All calculations in this session were performed using the Thresholdmodeling library in Python (Lemos et. al., 2020). The description of all calculations can be found in Coles (2001) where Statistical Modeling of Extreme Values is provided in detail.

For the application of the POT model, the threshold u must be determined, and for correct modelling, it is necessary to choose a suitable threshold; that is, one that is
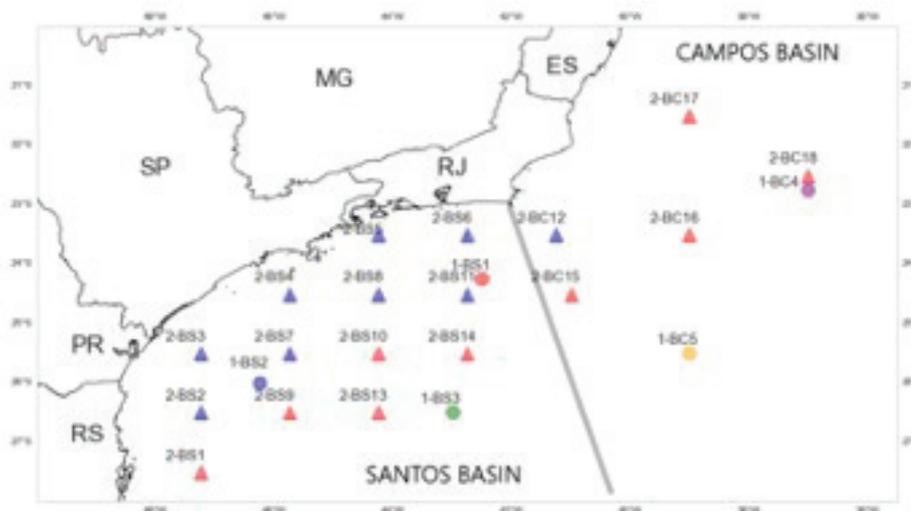
Figure 1. location of the 10 m wind (circle) and Hs (triangle) data points, where BS and BC are abbreviations for Santos Basin and Campos Basin respectively. 10 m wind points were chosen using a cluster analysis generated from the ERA 5 Reanalysis data, not shown in this paper. Hs points were chosen using 1° latitude and longitude spacing. The Hs points (triangles) in red are the points that were possible to calculate the return levels for all directions, the points in blue did not contain the minimum number of observations (at least 1 per year) in certain directions to perform the calculations

neither too large resulting in few surpluses and high variance, nor too small to generate bias in the modelling (Coles, 2001). Because of this, two methods are used to identify the threshold. The first method uses the analysis of the Mean Residual Life Plot and its linearity, where the smallest value within a given interval is selected as the threshold, from which the MRL has an approximately linear behaviour (Figure 2a).

From the beginning of the curve until approximately 7 it is possible to observe a decrease in the ordinate value and concave behaviour, not indicating a straight line, from 7 onwards this curved behaviour loses evidence.

Despite being very useful, it is common to have some kind of difficulty in interpreting the Mean Residual Live Plot, thus compromising the choice of u suitable. Therefore, a second method is applied, being complementary to the first, based on the stability of the parameters. In this case, if excesses above a threshold u_0 follow a GPD with parameters $\xi e \sigma$, then excesses above a threshold $u > u_0$ also follow a GPD with the same shape parameter .

$$\sigma_u = \sigma_{u0} + \xi(u - u_0) \qquad (1)$$

Then for $\xi \neq 0$, the scale parameter varies with u. However, by doing a reparameterization, in this case, $\sigma\ (u)$ is called the reparameterized scale parameter. The plots of $\sigma\ (u)$ and $\xi(u)$ have an apparent symmetry. The ICs for ξ are obtained from the variance-covariance matrix V. The ICs for $\sigma^\wedge$ require the use of the Delta Method. The smallest value within a given range should be selected as the threshold, after which the parameter is approximately constant and the points lose their linear behaviour and start to vary. (Figure 2b and 2c).

Thus, the choice of threshold should be made with the help of both methods. In the example, it is safe to say that the threshold is close to 7.

After choosing the appropriate threshold, the GPD parameters were calculated using the Maximum Likelihood Estimator (MLE).

One of the main goals of statistical inference is future forecasting. In dealing with extreme events, such analysis is necessary, given the impact generated by them. To obtain the return levels, the calculations explained below were performed.

Assuming that the GPD distribution is adequate to model the exceedances and having estimated the parameters σ, ξ by the MLE method, we easily obtain the following result:

$$P[X > u] = \zeta_u \qquad (2)$$

When $\zeta_u = P[X>u]$, i.e., the probability of exceeding the threshold. An empirical estimate of ζ_u can be given equation:

$$\zeta_u = \frac{N_u}{n} \qquad (3)$$

Where N_u is the number of observations exceeding the threshold u and n the total number of observations. Assuming that n measurements $X_1, X_2, ..., X_n$ were performed for N years obtaining $Y_1, Y_2, ..., Y_{Nu}$ iid exceedance observations, one can define n_y the number of exceedance observations per year. For the data, one can introduce the term "average exceedance rate", which is the average number of observations above the threshold u per year. Soon we can define the variable ζ_u as,

$$\hat{\zeta}_u = \frac{N_u}{n_y} \qquad (4)$$

Thus, the return period level x_m (which is exceeded on average once every m observations) is given by:

$$x_m = \begin{cases} \dfrac{u + \hat{\sigma}_u(\theta)}{\hat{\xi}(\theta)}\left[\left(\hat{\zeta}_u m\right)^{\hat{\xi}(\theta)} - 1\right], \xi(\theta) \neq 0, \\ u + \hat{\sigma}_u(\theta) log\left(\hat{\zeta}_u m\right), \xi(\theta) = 0, \end{cases} \qquad (5)$$

For the study of extremes, it is more convenient to provide return levels on an annual scale, so that the return level in N_y is the level that is expected to be exceeded on average once every N years. If there are n_y observations per years, this corresponds to the return level of m observations, where $m = N \times n_y$. Therefore, the return level of N_y is estimated using the equation:

$$x_N = \begin{cases} \dfrac{u + \hat{\sigma}_u(\theta)}{\hat{\xi}(\theta)}\left[\left(\hat{\zeta}_u N n_y\right)^{\hat{\xi}(\theta)} - 1\right], \xi(\theta) \neq 0, \\ u + \hat{\sigma}_u(\theta) log\left(\hat{\zeta}_u N n_y\right), \xi(\theta) = 0, \end{cases} \qquad (6)$$

To complete the analysis and generate the x_T, plots, the ranges of the CIs that were calculated using the Delta Method must be estimated. The uncertainties of ζ_u must also be included in the calculation. Finally, the return level curve is plotted, on a logarithmic scale, to emphasize the effect of extrapolation, as well as to add the CIs and empirical estimates of the return levels (Figure 2d).

Adhesion Tests

According to Zar (1998), to evaluate the level of agreement of a model to a data set one should perform adherence tests. Using the Thresholdmodeling library in Python, it was possible to verify that the statistical model describes the empirical observations well.

In statistics, a PP-Plot plot evaluates the agreement of two data sets, in the case of this study, the empirical data and theoretical data. So one way to interpret such a graph is to observe how distant these points are from this line, the more distant they are, the less suitable the proposed distribution is, so the data would not fit a GPD. In the same way, the QQ-Plot plot is evaluated.

Subsequently, the Kolmogorov-Smirnov Test, described in Campos (1983), was performed; it is a non-parametric method to test the fit of the distribution to the data, providing the conclusion whether the distribution is adequate or not.

The Dvoretzky-Kiefer-Wolfowitz Test limits how close a distribution function will be to the distribution function. This experiment was used to generate confidence bounds based on a Cumulative Distribution Function (CDF) to produce a confidence range, being parallel and equally spaced around the empirical CDP. For data to be modelled by a GPD, it must be close to the straight line and within the confidence band.

4. RESULTS AND DISCUSSION

This section presents the results and discussion of all variables analyzed. After the choice of threshold, the adherence tests were performed, to verify how well the data can be represented by a GPD. Finally, after all the tests, it was possible to obtain the return period levels x_N that were estimated by the POT Model for 100 years, using 99.9% statistical significance level.

Wind at 10 m

Through the adherence tests, it was possible to evaluate the quality of the data and whether it could be represented by a GPD. We present the resulting point 1-BS3 and selecting the SW direction to perform the adherence tests. Analyzing Figure 3, it is possible to see the consistency between the empirical data and model, with few values far from the straight line, but all within the CI. Thus, it is evident that the data are adequate to calculate the return level, and the results are similar for the other directions and points are chosen.

a)

b)

c)

d)
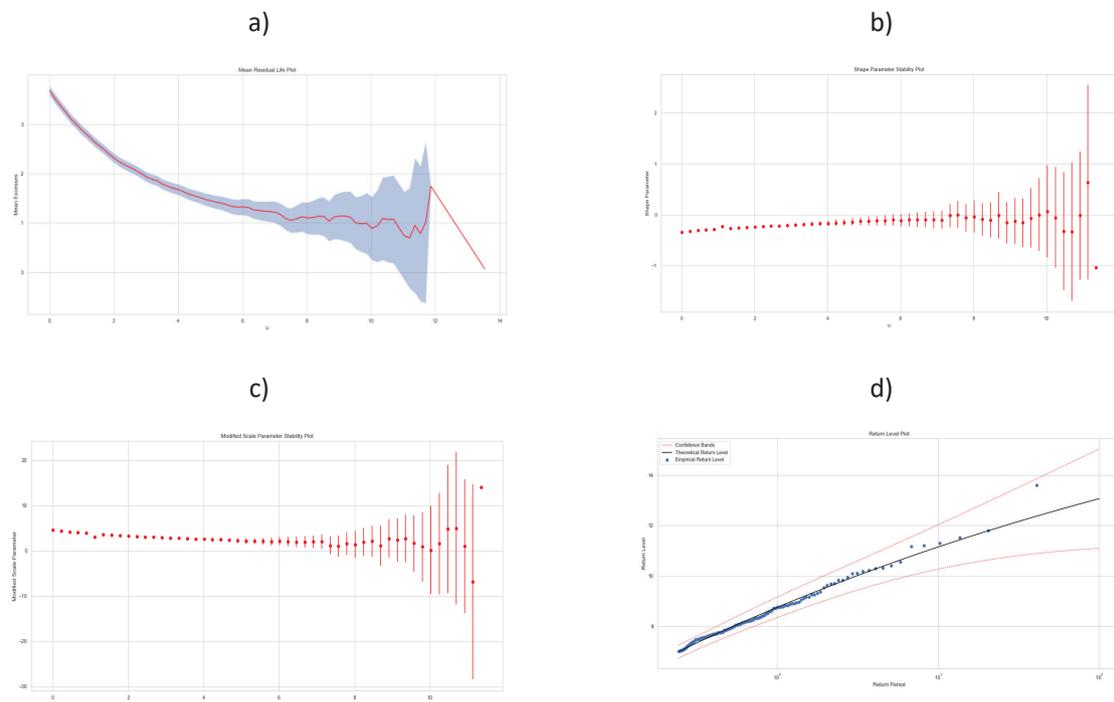
Figure 2. a) Mean Residual Live Plot. The Blue shaded area shows 99.9% confidence intervals. b) Shape Parameter Stability Plot. c) Modified Scale Stability Plot. In both plots the shape parameter and scale lose their linear behaviour at approximately 7. d) Return Level Plot with . The black solid line represents the theoretical return level (y-axis) up to 100 years return period (x-axis). Return levels from empirical data are represented by the blue dots. Red dashed lines represent the 99.9% point-to-point confidence interval.

Wind speed at 10 m

First, a preliminary analysis of the data was performed through descriptive statistics and the construction of Roses of Winds over a period of 41 years (1979-2019). Based on the data in Table 1, it can be seen that point 1-BS3 presents the highest values on average, although they are very close, and for this reason, the directional analysis is more valuable. In Figure 4a it can be seen that point 1-BS1, has a higher occurrence of winds from the NE quadrant, presenting lit-

tle occurrence of wind in other directions. However, from an analysis of the data, it was observed that the S direction obtained the maximum value of wind speed. At point 1-BS2 despite the NE winds having a higher frequency, there are significant occurrences of winds in other directions (Figure 4b). Highlighting the winds coming from S and SW that generated the maximum value of speed. The data from point 1-BS3 show a predominance of NE winds, this being a dominant characteristic in the study region (Figure 4c). Although the S and SW winds have a relevant amount of observations,
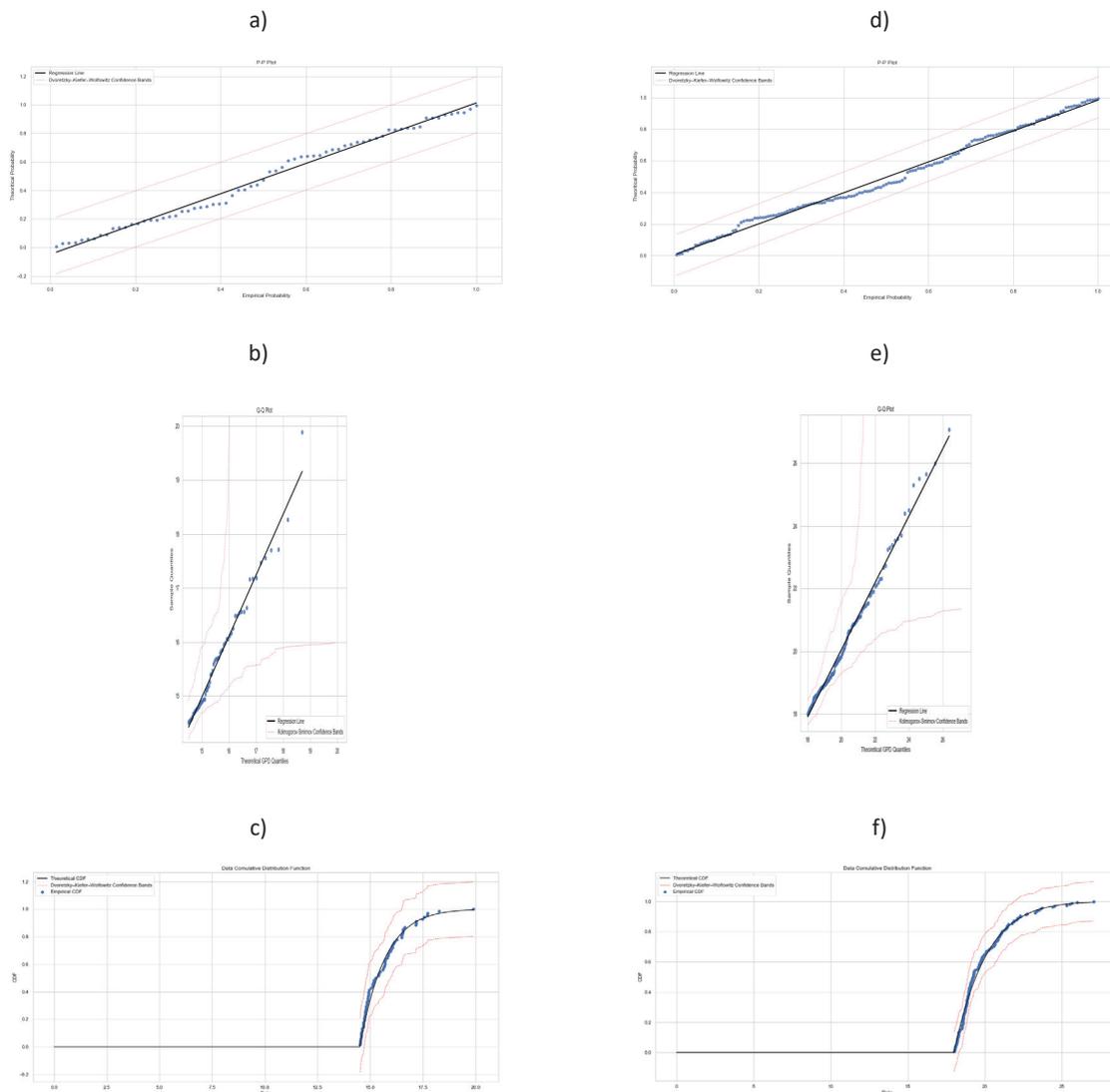
Figure 3. Adherence tests for modelling the GPD distribution for the time series of Point 1-BS3 and SW direction (a), b) and c) wind speed, d), e) and f) wind gust). In a) and d) the PP-Plot plot is shown where the y-axis represents the probability of the theoretical data and the x-axis of the empirical data. The black solid line represents the linear regression of the points and the red dashed line represents the 99.9% confidence interval calculated from the Dvoretzky-Kiefer-Wolfowitz Method. In b) and e) the QQ-Plot plot is shown, where the x-axis represents the quantiles of the empirical data and the y-axis, the quantiles of the theoretical data. The black solid line represents the linear regression of the points, and the red dashed line represents the 99.9% confidence interval calculated from the Kolmogorov-Smirnov Method. In c) and f) the Data Cumulative Distribution Function plots are shown. The solid line represents the theoretical data, the dots represent empirical data, and the red dashed line is the 99.9% confidence interval calculated from the Kolmogorov-Smirnov Method.

on average the NE winds have higher velocities at this point. However, the NW and S directions present the highest maximum values. At point 1-BC4 (Figure 4d), there is a higher occurrence of N and NE winds, and this one has the highest average value of wind speed. The W direction has the occurrence of the maximum value of the time series. Point 1-BC5 (Figure 4e), shows a higher occurrence of N and NE winds, being the one with the highest average and maximum wind speed value in the N direction. The SE direction also showed high maximum and average values.

The results obtained through the POT Model for the calculation of the wind return levels at 10 m and their respective CIs of 99.9% can be seen in Table 2.

At point 1-BS1, as can be seen, that the W direction has the highest value of and the E direction with the lowest value. From the Beaufort Scale, the winds were classified as Very Strong or force 8 in the S and W directions, and the other directions as Strong or Force 7 (except NW direction which has Force 6 or Very Cool). In 1-BS2 it is noted that it has SE with the highest values and N with the lowest values. The SW direction classified as Strength 11 or Stormy. The directions E, SE, S and SW can be classified as

Very Strong or Strength 8, the other directions as Strong or Strength 7.

Table 1. Descriptive statistics of the random variable wind speed at 10 meters (m/s) for the 41 years (1979-2019) of the points in Figure 1

Points	Mean (m/s)	Maximum (m/s)	Minimum (m/s)	Standard Deviation (m/s)
1-BS1	6.68	20.33	0.02	2.78
1-BS2	5.88	20.62	0.03	2.58
1-BS3	6.85	20.62	0.01	2.73
1-BC4	6.99	20.15	0.01	2.59
1-BC5	6.52	17.62	0.01	2.29

Already at point 1-BS3 presents the highest values of , being the S directional component with the highest value. Considering the CI, the NW direction has greater amplitude, this occurs because the CI at this point was greater for NW than for the S direction, with this the upper limit of NW generated higher values of return level. The N direction presented the lowest value for point 1-BS3. The NW
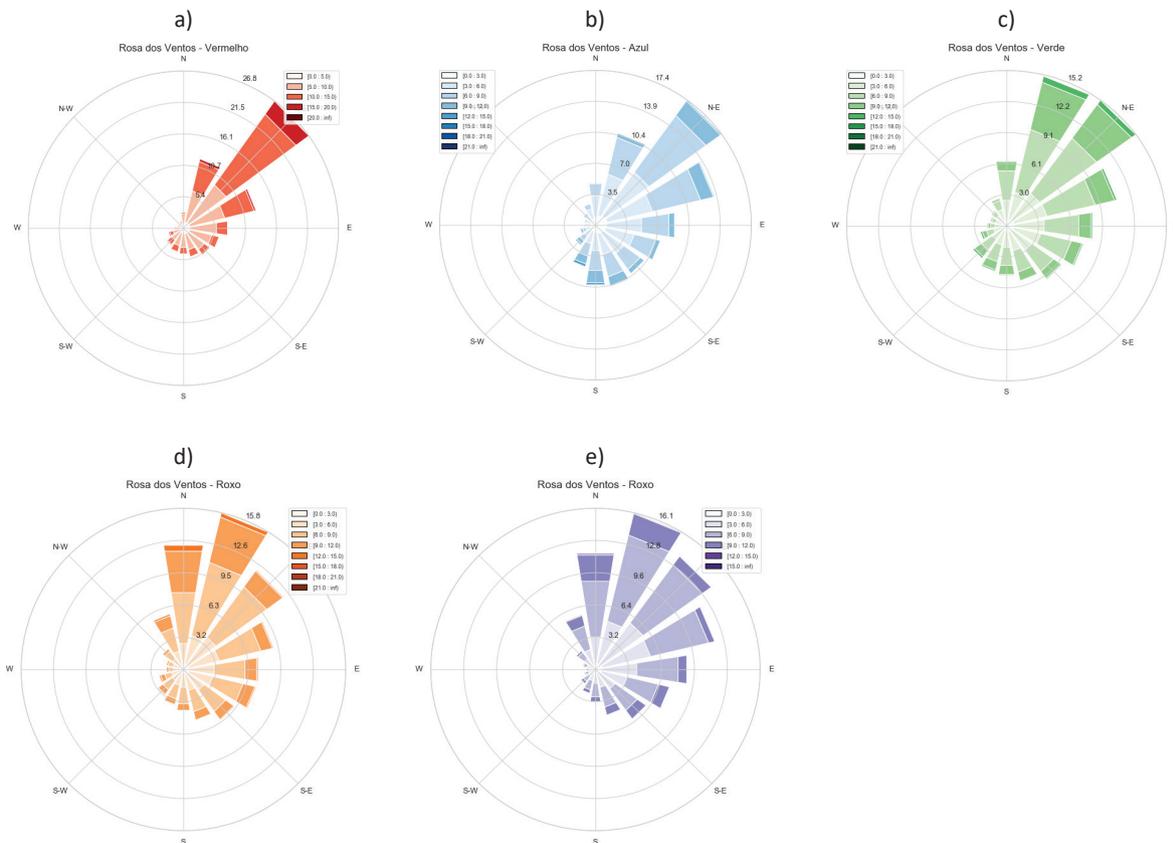
Figure 4. Wind roses depicting wind direction and speed at 10 m during the period 1979-2019 at the respective points a) 1-BS1 b) 1-BS2 c) 1-BS3 d) 1-BC4 e) 1-BC5.

and S quadrant winds were classified as Hard or Strength 9, and the other directions as Very Strong or Strength 8.

It can be seen that at point 1-BC4 the N and S directions have the highest values and the NW direction has the lowest value. All directions, from the Beaufort Scale, were classified as Very Strong or Strength 8. The result for point 1-BC5 shows values, the N direction has the highest value and the W direction the lowest value. Winds from N and NE directions can be classified as Very Strong or Strength 8, the other directions as Strong or Strength 7.

Prevailing atmospheric patterns

The predominance of winds in the Southwest Atlantic Ocean region is related to several factors. In the South Atlantic region, having a greater influence of the SAS - high-pressure centre with a length of approximately 2000 km - is constituted from the branch of the Hadley cell near 30ºS (Campos, 2009). The SASA has a semi-permanent character, contributing to the persistence of winds from the north and northeast quadrants, which result in meteorological phenomena in the region within the micro, meso and synoptic scales and can cause instability or stability according to their positioning and atmospheric composition. The prevailing SAS winds can undergo reversal to south quadrant winds when other synoptic scale phenomena reach the region (Silva, 2013). The transient atmospheric systems can make the weather unstable, such as lows, frontal systems, various types of cyclones, and other systems arising from ocean-atmosphere interaction that also promote intensification of winds, with gusts being the phenomenon of greatest destructive potential, because its exact prediction is still complex and uncertain. The incursion of a transient system implies changes in some meteorological variables, the main ones being: pressure, wind, temperature, humidity, cloud cover and precipitation. The wind is an important diagnostic component of the approach of these systems,

by the sudden change in its intensity and direction. In the South and Southeast regions of Brazil, the wind at low levels has a northeast predominance, as mentioned earlier, in a pre-frontal situation can be observed in the meteograms a turn in the wind that becomes southwest and southeast following the advance of the front (Vianello, 1991; Fedorova, 1999; Oliveira et al., 2001).

Another phenomenon present in the coastal region that can occasionally travel tens of kilometres is the breeze circulation, which is formed from the differential heating between the continent and ocean, generating temperature gradients that cause energy flows to the atmosphere, responsible for the formation of pressure gradients that drive the movement. The sea breeze, under stable synoptic conditions, increases wind intensity, changes its direction and transports moisture, and may be responsible for some events that generate extreme conditions in the coastal region (Atkinson, 1981). In Silva (2013) it was found a core amount of values above the threshold on the southeast coast (around the region of Cabo Frio-RJ), indicating to be an area with a greater amount of values above the threshold for the NE direction. This can be observed in Figure 10 where all the points of this study, especially the redpoint, indicate the greatest amount of observations coming from the NE direction. However, this is not the direction that returns the highest extreme values, which was also observed in Silva (2013), being the highest return levels for the southeast region of Brazil resulting from the SE, S and NW directions. It can be seen that in this study the highest values are also found in these directions, highlighting the point 1-BS3 that presented the S direction with the highest return level of the three points.

Wind Gust at 10 m

Based on the data in Table 3, we have that point 1-BS3 presented on average the highest values; however, point

Table 2. Table 100-year Return Level Values of the variable Wind at 10 m for points 1-BS1, 1-BS2, 1-BS3, 1-BC4 and 1-BC5.

Direction	1-BS1			1-BS2			1-BS3			1-BC4			1-BC5		
	x_N	$+IC_9$	$-IC_9$	x_N	$+IC_9$	$-IC_9$	x_N	$+IC_9$	$-IC_9$	x_N	$+IC_9$	$-IC_9$	x_N	$+IC_9$	$-IC_9$
N	15.51	17.69	13.33	14.39	15.36	13.41	17.73	19.47	15.98	19.45	21.78	17.12	17.43	19.64	15.22
NE	16.55	17.79	15.31	15.67	16.70	14.63	19.25	21.82	16.67	18.35	20.78	15.91	18.30	22.47	14.14
NW	13.07	15.05	11.10	16.55	18.64	14.46	21.04	28.06	14.02	17.99	20.17	15.80	15.27	16.28	14.26
S	18.23	20.40	16.05	19.92	23.73	16.10	21.25	26.26	16.25	19.44	22.77	16.10	17.04	19.41	14.69
SE	16.21	17.94	14.47	20.63	26.35	14.92	17.75	19.14	16.36	18.24	21.38	15.11	17.03	19.50	14.57
SW	16.86	17.73	15.99	19.64	22.03	17.24	19.76	22.68	16.84	18.51	21.33	15.70	15.12	15.81	14.44
E	15.56	16.82	14.32	17.42	19.75	15.10	20.29	23.49	17.10	19.01	22.72	15.30	16.88	20.79	12.97
W	18.41	21.31	15.51	17.04	18.76	15.33	20.13	22.36	17.91	19.29	21.42	17.16	14.97	16.89	13.06

1-BS2 presented the highest maximum value. The standard deviation and variance obtained similar values, being higher if compared to the wind speed presented in the previous section. Figure 5 shows the data represented in a wind rose graph. As observed in the statistical analysis of the Wind Speed at 10 m, all points indicated a higher occurrence of winds coming from NE. From an analysis of the maximum values (Table 3), the point 1-BS1 showed the S direction with the highest value, the point 1-BS2 showed the NE direction with the highest value and the point 1-BS3 showed the E, SE and W directions with the highest values what was not observed in the analysis of the respective wind speeds at 10 m in the three points. Point 1-BC4 is represented in Figure 5d, where it is observed a higher occurrence of N and NE winds, having the highest average values. By statistical analysis, it was found that the highest value of the gust occurred in the SW direction, which also did not occur for wind speed at 10 m. In Figure 5e we note that point 1-BC5 has the largest number of observations in the NE and N direction, and maximum value in the S direction where, again, was not observed in the wind speed at 10 m.

The values of return levels and their respective 99.9% CIs can be seen in Table 4.

It is observed at point 1-BS1 that the W direction has the highest value of and the NW direction with the lowest value. From the Beaufort Scale, the winds are classified as Hard or Force 9 in all directions except NW as Very Strong or Force 8.

Table 3. Descriptive statistics of the random variable wind gust at 10 meters for the 41 years (1979-2019) (m/s) of the points in Figure 1.

Points	Mean (m/s)	Maximum (m/s)	Minimum (m/s)	Standard Deviation (m/s)
1-BS1	9.06	24.67	0.54	3.53
1-BS2	7.94	30.78	0.18	3.32
1-BS3	9.25	29.58	0.29	3.49
1-BC4	9.41	27.06	0.59	3.27
1-BC5	8.85	24.66	0.92	2.84
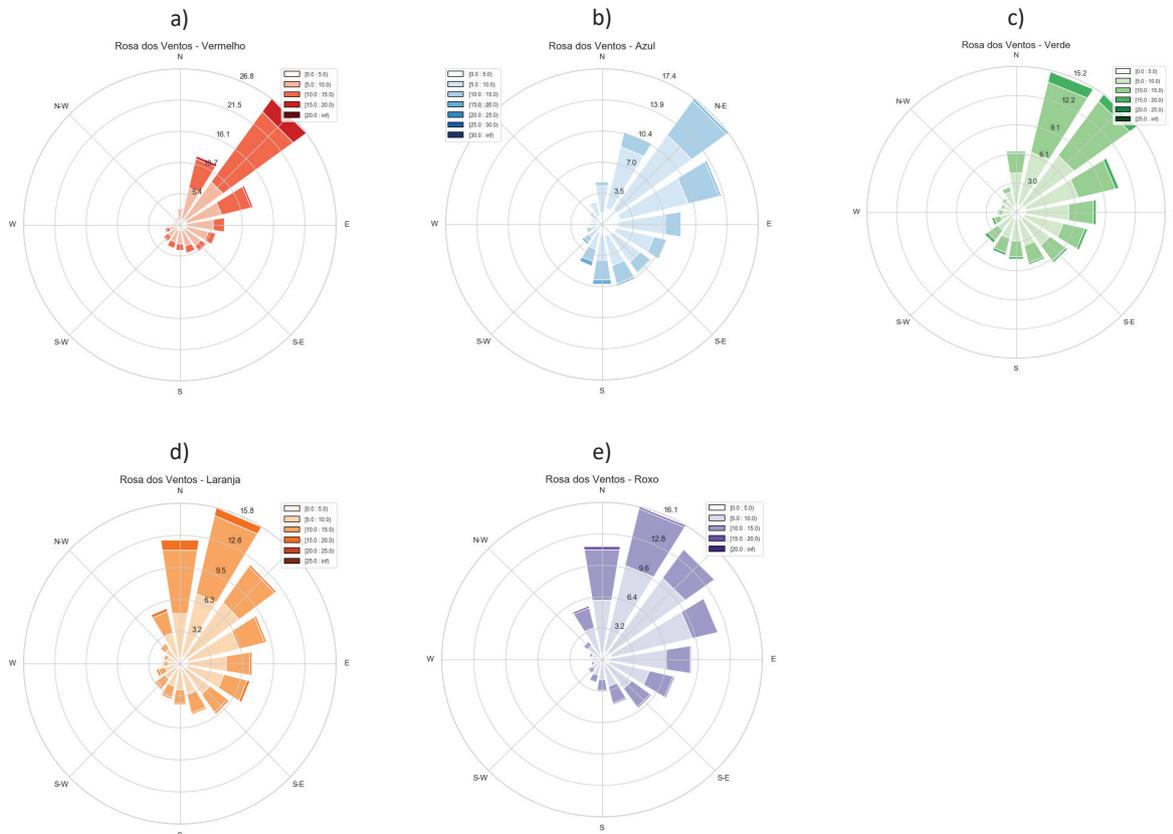
Figure 5. wind rose representing wind direction and gust at 10 m during the period 1979-2019 at the respective points a) 1-BS1 b) 1-BS2 c) 1-BS3 d) 1-BC4 e) 1-BC5

From the result of point 1-BS2, it is noted that it has SW with the highest values and N with the lowest values. The S and SW directions classified as Stormy or Strength 11, the W direction as Very Hard or Strength 10, the other directions as Hard or Strength 9.

Point 1-BS3 presented on average the highest values, with the E direction having the highest value. The NE direction presented the lowest value. The E and W quadrant winds are classified as Stormy or Force 11, the N, NW, S, SE and SW directions as Very Hard or Force 10 and the NE direction as Hard or Force 9.

For the Campos Basin, points 1-BS4 and 1-BC5 were used. Point 1-BS5 presents the S direction with the highest and the E direction with the lowest value. The S quadrant winds are classified as Stormy or Force 11, the NW, N, SW and W directions as Very Hard or Force 10 and the E and SE directions as Hard or Force 9. At point 1-BC4 the SE direction has the highest value of and the SW direction the lowest value. The SW direction is Very Hard or Strength 8, and the other directions as Hard or Strength 9.

The work of Liska et al. (2013a) aimed to estimate the maximum wind speed levels for the municipality of Piracicaba-SP and compare the results of two methodologies: Maximum blocks and the POT. The results showed that the POT was more accurate since it presented lower values of relative standard error. In the studied period, the highest estimated return level was 29.39 m/s for 100 years, which is considered, from the Beaufort Scale, as Stormy or Force 11.

In the study by Sant'Anna (2018), the procedures for the estimation of extreme winds, currently used in France, are presented. To obtain the 50-year return level values, the POT statistical model and the wind gust velocity database for the state of Rio de Janeiro were used. It can be seen that in the present study the values are also between 20 and 30 m/s,

the highest value being 29.81 m/s at point 1-BC4. If the CI is considered, the return level reaches 38.64 m/s, at the same point, for the S direction.

Significant Wave Height

Figure 6 shows the graphs of the adherence tests of the data to the model. Point 2-BS14 was chosen and the SW and W directions were selected. It is possible to see the coherence of the model in representing the empirical data since the values are close to the straight line and within the CI. It is concluded that the model and the Hs data can be represented by a GPD, therefore the level of return can be calculated.

Based on the data in Table 5, point 2-BS13 presents an average of 2.01 m of Hs and a maximum value of 7.08 m, which comes from the SW. At point 2-BC15 a maximum value of 6.02 m from SW is observed.

It can be seen from Figures 7a and 7b that the S, SE, E and NE directions have the most observations.

Figure 8 shows a map where the respective wind rose was generated for each point. From it, one can better visualize the data and conclude that the region has a higher occurrence of waves coming from the NE, E SE, S and SW directions.

The results obtained through the POT Model to calculate the levels of return for the variable Hs and their respective 99.9% CIs can be seen in Tables 6 to 9. They are presented in the form of graphs (Appendix) and tables.

Point 2-BS13 presents, on average, the largest values of , with the largest value belonging to the SW direction at this point. The point 2-BS4 presents on average the lowest values of , being the N direction the lowest value.

Table 4. Table 100-year Return Level Values of the variable Wind Gust at 10 m for points 1-BS1, 1-BS2, 1- BS3, 1-BC4 and 1-BC5.

Direction	1-BS1			1-BS2			1-BS3			1-BC4			1-BC5		
	x_N	$+IC_9$	$-IC_9$	x_N	$+IC_9$	$-IC_9$	x_N	$+IC_9$	$-IC_9$	x_N	$+IC_9$	$-IC_9$	x_N	$+IC_9$	$-IC_9$
N	22.24	25.00	19.52	21.29	23.42	19.16	25.61	29.38	21.85	27.93	31.48	24.39	23.10	26.05	20.16
NE	22.44	23.41	21.46	22.82	25.04	20.59	24.55	26.49	22.60	26.46	30.30	22.62	23.12	27.17	19.07
NW	18.00	20.15	15.65	21.54	24.83	18.24	25.50	28.84	22.16	25.34	29.63	21.04	21.51	23.34	19.68
S	25.46	33.54	17.39	28.24	34.14	22.33	28.44	33.36	23.51	29.81	38.64	20.98	23.86	28.33	19.39
SE	22.06	24.50	19.63	27.80	34.12	21.49	26.54	30.41	22.67	24.47	28.41	20.52	23.89	28.45	19.33
SW	23.45	24.91	22.00	29.56	37.06	22.06	28.01	32.09	23.93	26.69	30.17	23.21	20.27	21.27	19.26
E	21.53	23.46	19.61	23.70	26.33	21.08	29.32	34.17	24.47	24.36	27.21	21.50	23.25	28.17	18.33
W	26.79	30.90	22.49	25.42	28.67	22.17	29.07	32.37	25.76	26.52	29.62	23.43	21.72	26.15	17.29
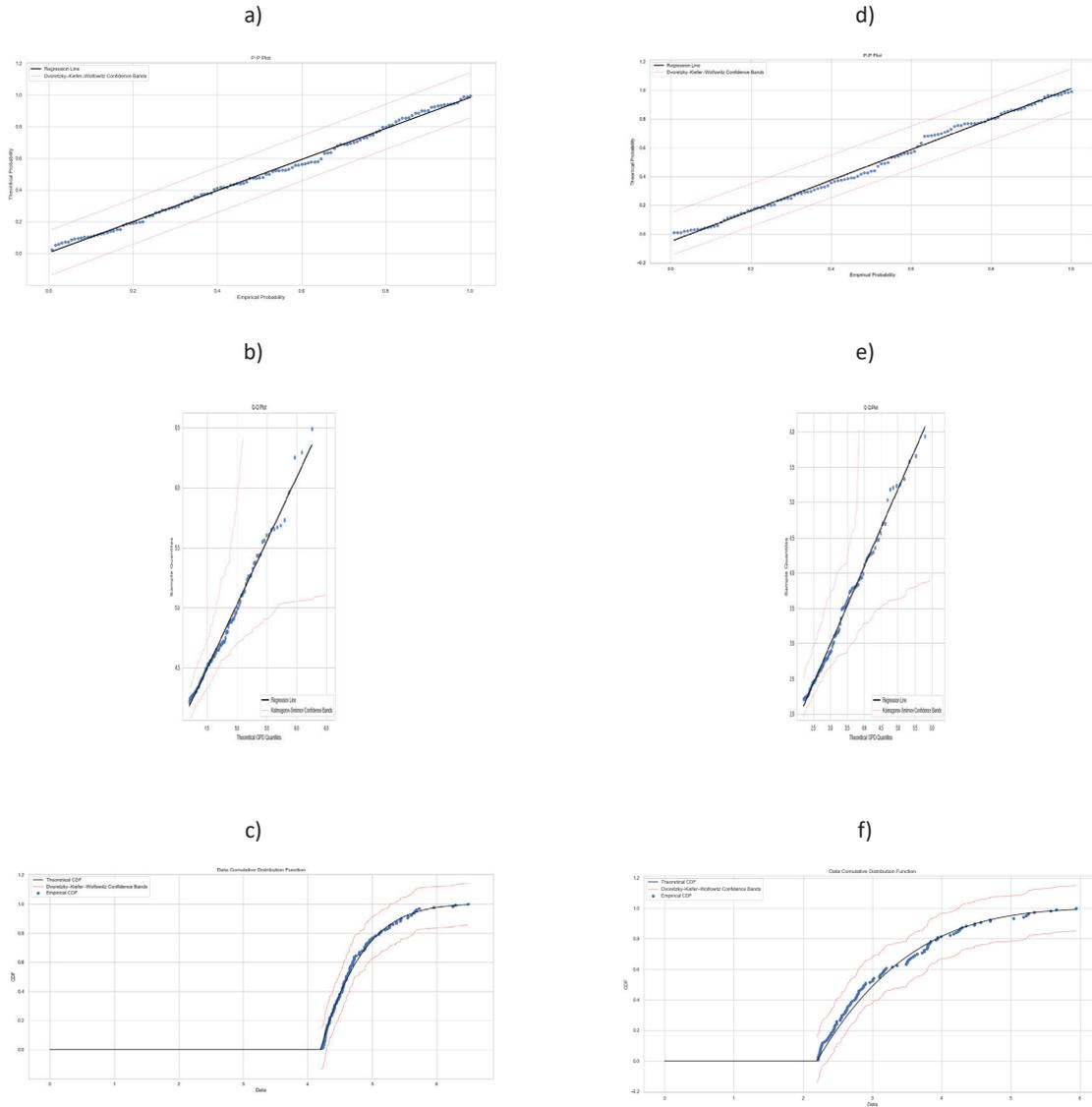
Figure 6. Figure exposing the tests of adherence for modelling the GPD distribution for the time series of the variable Hs from Point 2-BS14 and direction SW(a), b) and c)), and direction W (a), b) and c)). In a) and d) the PP-Plot plot is shown where the y-axis represents the probability of the theoretical data and the x-axis of the empirical data. The black solid line represents the linear regression of the points, and the red dashed line represents the 99.9% confidence interval calculated from the Dvoretzky-Kiefer-Wolfowitz Method. In b) and e) the QQ-Plot plot is shown, where the x-axis represents the quantiles of the empirical data and the y-axis, the quantiles of the theoretical data. The black solid line represents the linear regression of the points, and the red dashed line represents the 99.9% confidence interval calculated from the Kolmogorov-Smirnov Method. In c) and f) the Data Cumulative Distribution Function plots are shown. The solid line represents the theoretical data, the dots represent the empirical data, and the red dashed line is the 99.9% confidence interval calculated from the Kolmogorov-Smirnov Method.

Table 5. Descriptive statistics of the random variable Hs (m).

Point	Mean (m/s)	Maximum (m/s)	Minimum (m/s)	Standard Deviation (m/s)
2-BS1	1.89	7.13	0.61	0.65
2-BS2	1.77	6.89	0.60	0.59
2-BS3	1.61	5.63	0.54	0.51
2-BS4	1.65	5.47	0.57	0.52
2-BS5	1.56	4.94	0.51	0.50
2-BS6	1.78	5.46	0.66	0.53
2-BS7	1.82	6.45	0.65	0.59
2-BS8	1.84	5.96	0.68	0.57
2-BS9	1.93	7.03	0.65	0.64
2-BS10	6.38	6.38	0.70	0.61
2-BS11	1.96	6.08	0.73	0.57
2-BC12	1.96	5.62	0.72	0.53
2-BS13	2.01	7.08	0.69	0.64
2-BS14	2.03	6.49	0.76	0.60
2-BC15	2.03	6.02	0.78	0.57
2-BC16	1.99	5.87	0.82	0.55
2-BC17	1.87	5.01	0.80	0.50
2-BC18	1.93	5.38	0.77	0.54

Parente (1999) studied the weather systems and related them with the sea condition in the Campos Basin, defining four main categories: Good Weather, Good Weather with swells, Bad Weather - southwest storm and Bad Weather - southeast storm.

The Good Weather situations are characterized by the dominance of SASAS where the wind is predominantly from NE. Thus, it produces a local sea in the same direction as the winds (Figure 9a). However, in situations of local SASAS, there may also be swells coming from high latitudes, characterizing the sea condition as Good Weather with swells (Figure 9b). The frontal systems (fronts with associated extra-tropical cyclones) when they move near the coastal area of Southeast Brazil are responsible for the most severe oceanic condition, generating the largest Hs coming from the southwest and south, characterizing sea condition of Bad Weather - storm from the southwest.

The extratropical or polar anticyclones (highs in the rear of the cold fronts) can intensify the southeasterly winds, especially when the displacement of the extratropical cyclone decreases or sometimes stops, causing the anticyclone to dominate the circulation, characterizing the sea condition as Bad Weather - southeast storm. This configuration (Figure 9c) generates a track, intensity and persistence of winds favourable for the formation of swells that may eventually propagate to the coastal region of southeastern Brazil (Figure 9d), and provoke southeast swell phenomena. This was detected by Innocentini and Caetano Neto (1996) where the high swells caused great damage and at least one death reported by the media in 1988. A similar more recent configuration in which the swells were able to enter Guanabara Bay in 2019, the Hs was approximately 3.5 m. (Mazzaro et al., 2019) [Figure 9c and 9d].

a)   b)
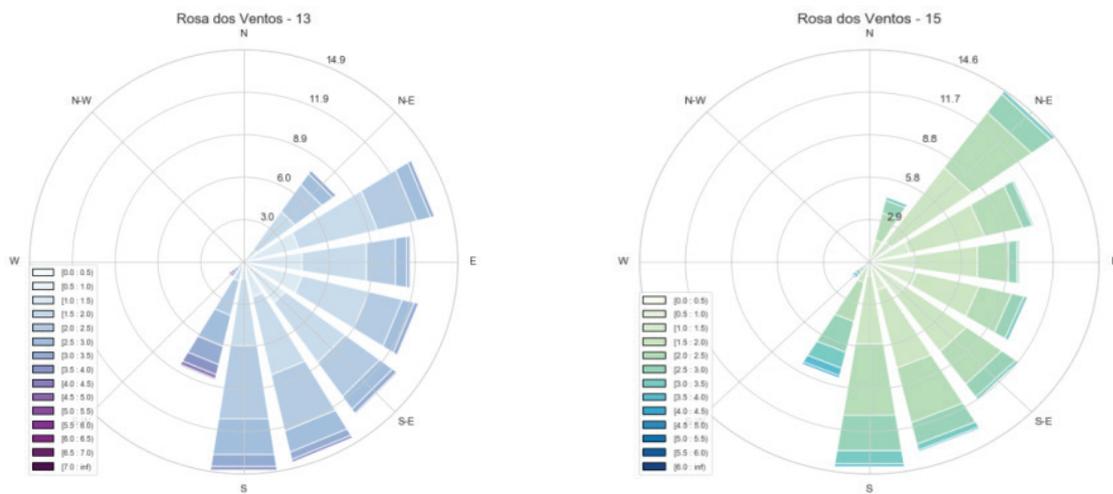
Figure 7. a) Wind roses representing Hs. direction (a) at point 2-BS13 and (b) at point 2-BC15 during the period 1979-2019.
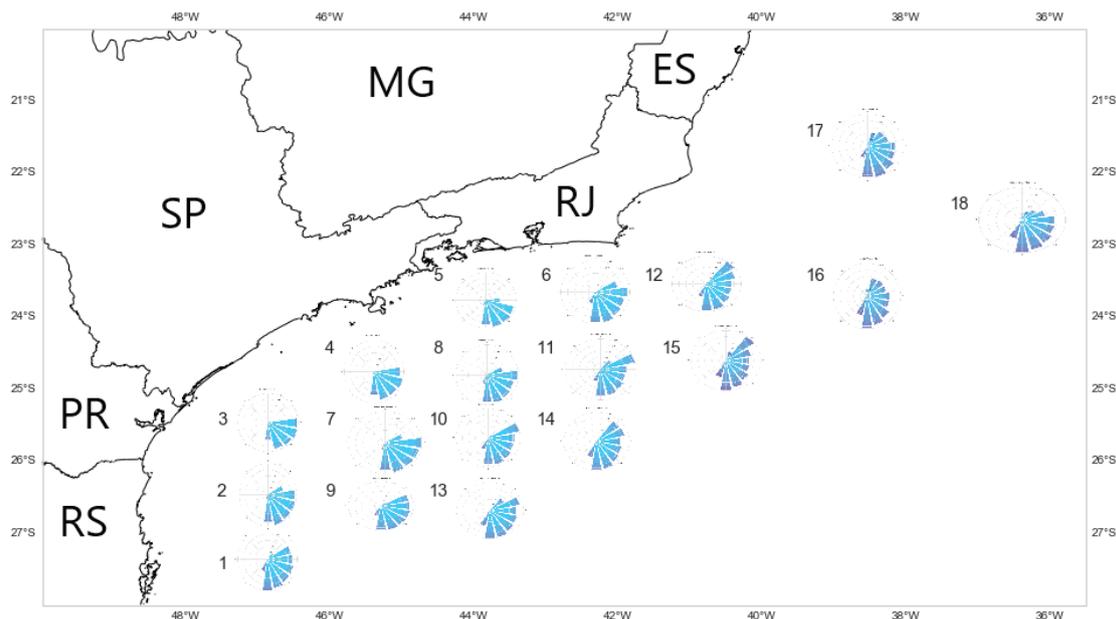
Figure 8. Location on the map of the Hs points and their respective Wind Rose for the period 1979-2019.

Table 6. 100-year Return Level values of the variable Significant Wave Height for points 2-BS1, 2-BS2, 2-BS3, 2-BS4, and 2-BS5.

Direction	2-BS1			2-BS2			2-BS3			2-BS4			2-BS5		
	x_N	$+IC_9$	$-IC_9$	x_N	$+IC_9$	$-IC_9$	x_N	$+IC_9$	$-IC_9$	x_N	$+IC_9$	$-IC_9$	x_N	$+IC_9$	$-IC_9$
N	3.48	3.83	3.13	3.58	3.77	3.38	3.07	3.40	2.75	2.38	2.54	2.22	-	-	-
NE	4.67	5.14	4.21	-	-	-	-	-	-	-	-	-	-	-	-
NW	3.80	4.26	3.35	-	-	-	-	-	-	-	-	-	-	-	-
S	7.39	8.24	6.54	6.51	7.34	5.67	5.55	6.40	4.70	5.50	6.19	4.82	5.15	5.93	4.37
SE	6.49	8.08	4.90	5.30	5.72	4.87	4.89	5.53	4.24	4.14	4.34	3.93	4.02	4.20	3.84
SW	7.75	8.85	6.66	5.73	6.15	5.32	4.89	5.53	4.24	5.17	5.71	4.64	4.88	5.17	4.60
E	5.51	6.32	4.69	4.88	5.45	4.32	4.33	4.80	3.86	4.11	4.40	3.82	3.60	3.84	3.37
W	3.86	4.24	3.47	-	-	-	-	-	-	-	-	-	-	-	-

Table 7. 100-year Return Level values of the variable Significant Wave Height for points 2-BS6, 2-BS7, 2-BS8, 2-BS9 and 2-BS10.

Direction	2-BS6			2-BS7			2-BS8			2-BS9			2-BS10		
	x_N	$+IC_9$	$-IC_9$	x_N	$+IC_9$	$-IC_9$	x_N	$+IC_9$	$-IC_9$	x_N	$+IC_9$	$-IC_9$	x_N	$+IC_9$	$-IC_9$
N	3.17	3.35	2.99	4.06	4.36	3.76	3.66	3.82	3.53	3.39	3.71	3.00	3.21	3.47	2.97
NE	-	-	-	-	-	-	-	-	-	4.48	4.82	4.14	4.37	4.60	4.14
NW	-	-	-	-	-	-	-	-	-	4.63	6.00	3.27	4.10	5.07	3.14
S	5.01	5.42	4.60	6.53	7.65	5.40	5.73	6.59	4.89	6.38	6.84	5.90	5.78	6.23	5.33
SE	4.26	4.44	4.08	4.93	5.30	4.55	4.53	4.75	4.32	5.73	6.20	5.27	4.82	5.06	4.57
SW	5.47	5.75	5.19	6.46	7.24	5.66	6.03	6.55	5.51	7.20	7.76	6.64	6.58	7.06	6.10
E	4.68	5.68	3.67	4.56	4.92	4.20	4.60	5.00	4.21	5.43	6.09	4.77	5.04	5.60	4.48
W	-	-	-	-	-	-	-	-	-	5.88	7.13	4.63	5.72	6.72	4.71

Table 8. 100-year Return Level values of the variable Significant Wave Height for points 2-BS11, 2-BC12, 2-BS13, 2-BS14, and 2-BC15.

Direction	2-BS11			2-BC12			2-BS13			2-BS14			2-BC15		
	x_N	$+IC_9$	$-IC_9$	x_N	$+IC_9$	$-IC_9$	x_N	$+IC_9$	$-IC_9$	x_N	$+IC_9$	$-IC_9$	x_N	$+IC_9$	$-IC_9$
N	4.33	4.75	3.92	4.29	4.85	3.73	5.14	4.86	3.42	3.85	4.33	3.37	4.48	5.03	3.94
NE	-	-	-	-	-	-	5.49	6.91	4.08	4.94	4.81	4.06	4.59	5.17	4.01
NW	-	-	-	-	-	-	5.05	6.12	3.98	3.92	4.46	3.37	3.41	3.61	3.22
S	5.51	6.05	4.96	5.19	5.56	4.82	6.89	7.96	5.82	6.03	6.56	5.50	5.78	6.26	5.29
SE	4.81	5.20	4.42	4.50	4.76	4.26	5.71	6.16	5.26	4.97	5.22	4.71	4.72	4.96	4.47
SW	6.06	6.43	5.69	5.82	6.37	5.27	7.77	8.97	6.56	6.57	7.07	6.07	6.25	6.89	5.62
E	4.51	5.00	4.03	4.76	5.28	4.25	5.97	7.11	4.83	5.08	5.64	4.53	4.91	5.54	4.28
W	5.17	5.80	4.54	4.34	5.37	3.31	6.63	7.44	5.83	6.26	7.15	5.38	6.28	7.64	4.91

Table 9. 100-year Return Level values of the variable Significant Wave Height for points 2-BS11, 2-BC16, 2-BC17, and 2-BC18.

Direction	2-BC16			2-BC17			2-BC18		
	x_N	$+IC_9$	$-IC_9$	x_N	$+IC_9$	$-IC_9$	x_N	$+IC_9$	$-IC_9$
N	4.56	4.97	4.15	3.82	4.12	3.52	3.82	4.12	3.52
NE	4.39	5.00	3.79	4.64	5.95	3.34	4.64	5.95	3.34
NW	4.21	4.73	3.69	3.82	4.41	3.23	3.82	4.41	3.23
S	5.81	6.85	4.78	5.07	5.50	4.64	5.07	5.50	4.64
SE	4.83	5.18	4.47	5.72	7.28	4.14	5.72	7.28	4.14
SW	5.91	6.57	5.25	5.17	5.68	4.65	5.17	5.68	4.65
E	5.03	5.95	4.10	4.35	5.03	3.67	4.35	5.03	3.67
W	4.34	4.80	3.88	3.73	4.26	3.20	3.73	4.26	3.20

Campos (2009) used the measurements of an ondograph located in the Campos Basin, between 1991 and 1995, and twenty years of simulation of the WAVEWATCH III model between 1986 and 2005, forced with winds from NCEP/NCAR Reanalysis to characterize the region. As a result, he obtained through the waveform data, that the largest swells were from SW with Hs of 9.54 m but with great uncertainty due to the short duration of the time series. The POT applied to the WAVEWATCH III data showed that the largest swells were caused by cyclones, resulting in a return level of 100 years with Hs around 7.884 m.

However, in the results found here, analyzing the waves in the Santos and Campos Basin, it was found that the largest swells were from SW in most points, except for points 2-BS2, 2-BS3, 2-BS4, 2-BS5 and 2-BS7 because they are closer to the coast. Nevertheless, they present the highest values in the S direction. It is worth mentioning that these results are in agreement with the methodology presented by Parente (1999).

5. CONCLUSIONS

First, adherence tests were performed, in which the results showed that the set of wind and wave data from the ERA5 reanalysis have an adequate consistency with the POT model. Based on this finding, it was possible to use it to calculate the 100-year return level of the variables studied.

As the applied technique needs great interactivity with the user, through the choice of thresholds, based on the analysis of the numerous graphs, the results become more accurate and less susceptible to errors. In some points, the wave extreme was not possible to be calculated for certain directions, for not having enough data for the calculation.

Through the POT Model, it was possible to conclude that the point 1-BS3 generated the highest value of wind speed of all points, in the S direction with a value of 21.25 m/s, considering a +IC 26.26 m/s. Point 1-BC4 generated the highest concerning the gust, with values of 29.81 m/s and +IC 38.64 m/s.

a)

b)

c)

d)
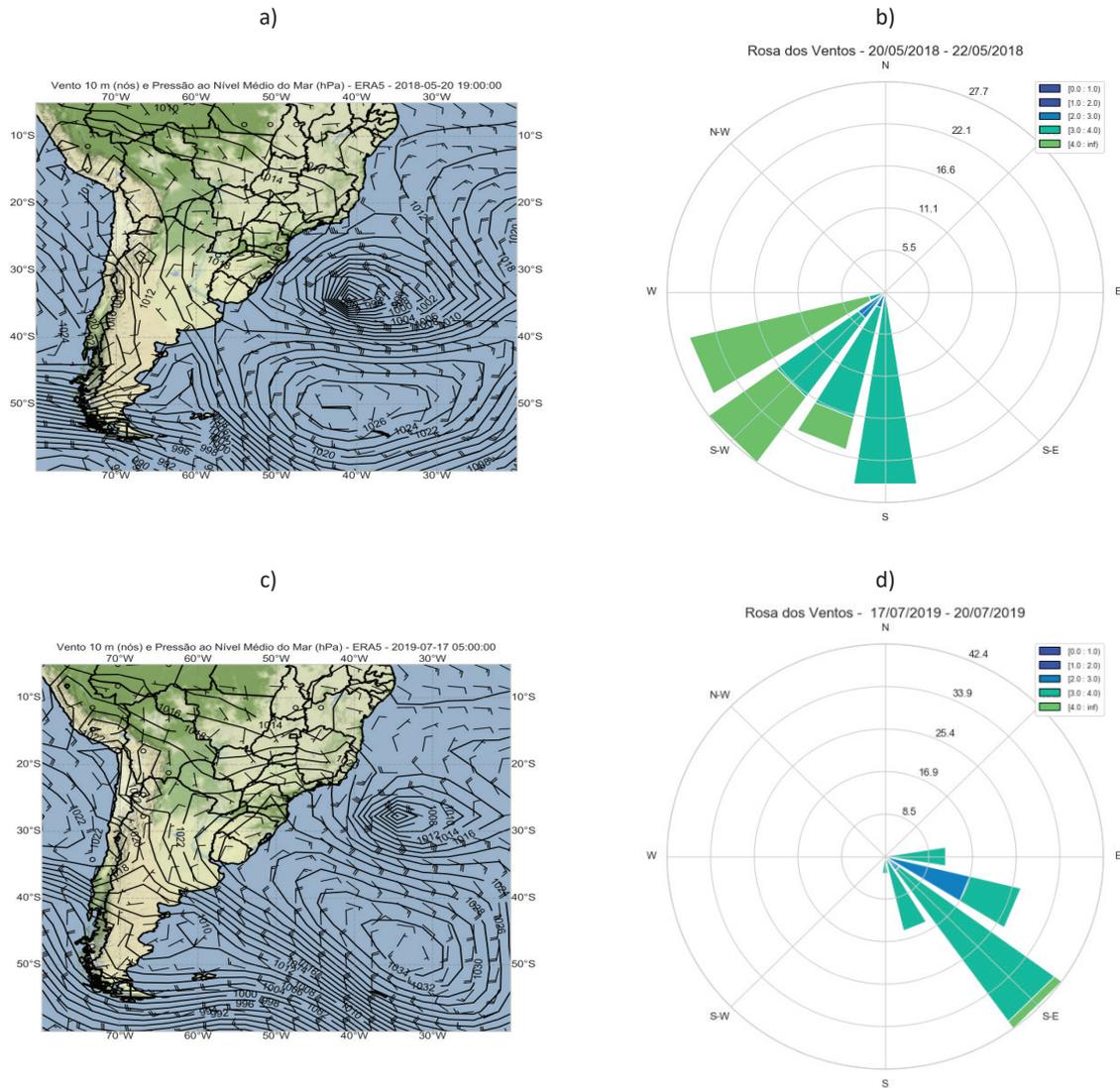
Figure 9. a) Wind at 10 m (knots) and Sea Level Pressure (hPa) - ERA5 from 05/20/2018 at 19z. b) Rose of Winds representing Hs and Average Wave Direction at point 2-BS10 from 05/20/2018 to 05/22/2018. c) Wind at 10m (knots) and Sea Level Pressure (hPa) - ERA5 from day 17/07/2019 at 05z. d) Wind rose to represent Hs and Average Wave Direction at point 2-BS10 from day 17/07/2019 to day 20/07/2019.

Analyzing the statistics of the data of the Wind points at 10 m, through the Wind Rose Graph it is possible to state that all points have a higher occurrence of NE winds, related to the activity of SAS in the region. The statistical analysis led to the conclusion that points 1-BS1 and 1-BS3 have higher values in average wind speed and gust at 10 m in the NE direction. Points 1-BC4 and 1-BC5 in the N direction, and only point 1-BS2 have, on average, the S direction with the highest values. This probably occurs because point 1-BS2 is more influenced by the geographic barrier, because it is closer to the continent, and consequently has less occurrence of winds coming from SAS when compared to the other points. The fact that the S direction has the highest average value is related to the fact that the region is influenced by the passage of frontal systems, which eventually move eastward, not reaching lower latitudes.

It is possible to conclude that from the statistics of data from points 13 and 15 of Hs, the largest swells that reach the BC and BS are those coming from SW, generated by frontal systems, occurring in situations of bad weather, as was found by Parente (1999). It is worth mentioning that this SW configuration occurs due to the contribution of the rear polar masses (high-pressure system) associated with cyclones, which increase the pressure gradient, the track and persistence of winds. By statistical analysis, the highest mean values at the two points also come from SW. The highest value of was found at point 13 in the SW direction with Hs of 7.77 m and considering the +IC 8.97 m.

Given the importance of this theme, the methodology used is effective to evaluate extreme values in the region. It is worth noting that, although data collected in situ are preferable when conducting a study, the use of ERA5 Reanalysis is an alternative to its use in locations that do not have a sufficiently long and consistent time series.

REFERENCES

Abild, J., Mortensen, N. G. & Landberg, L. (1992), *Application of the Wind Atlas method to extreme wind speed data*. J. Wind Eng. Ind. Aerodyn., pp. 41–44, pp. 473–484.

Andersson E, Thepaut JN. (2008), *ECMWF's 4D-Var data assimilation system – the genesis and ten years in operations*. ECMWF Newsletter Vol. 115, pp. 8–12.

ANP – Agência Nacional do Petróleo, Gás e Biocombustível, disponível em http://www.anp.gov.br/, acesso em 27 abr. 2020.

ANA – Agência Nacional de Águas. Disponível em: https://www.ana.gov.br/, acesso em: 27 abr. 2020.

Atkinson, B.W. *Meso-scale atmospheric circulations*. London, Academic Press, 1981. 495p., Chap. 5 e 6.

Babanin, A.V.; Rogers, W.E.; Camargo, R. de.; Doble, M.; Durrant, T.; Filchuk, K.; Ewans, K.; Hemer, M.; Janssen, T.; Kelly-Gerreyn, B.; Machutchon, K.; McComb, P.; Qiao, F.; Schulz, E.; Skvortsov, A.; Thomson, J.; Vichi, M.; Violante-Carvalho, N.; Wang, D.; Waseda, T.; Williams, G. and Young, I.R. (2019), Waves and Swells in High Wind and Extreme Fetches, Measurements in the Southern Ocean. Front. Mar. *Sci.* Vol. 6, p. 361.

Bjerknes, J. (1919), *On the structure of moving cyclones*. Geofysiske Publikasjoner, Vol. 1, No. 2, p. 1-8.

Campos, R. M. (2009), Análise dos Extremos de Onda no Rio de Janeiro Associados a Ciclones Extratropicais no Atlântico Sul. Dissertação (Mestrado) — Universidade Federal do Rio de Janeiro, Engenharia Oceânica. Universidade Federal do Rio de Janeiro.

Candella, R. (1997), Estudo de Alguns Casos Significativos de Ondas do Atlanfico Sul através de Modelagem Numérica. Tese de Mestrado, PEnO/COPPE/U FRJ, Rio de Janeiro, RJ, Brasil.

Candella, R. N.; Souza, S. M. L. (2013), Ondas oceânicas extremas na costa sul-sudeste brasileira geradas por ciclone com trajetória anormal em maio de 2011. *Revista Brasileira de Meteorologia*, Vol.28, No. 4, pp. 441-456.

Coles, S. (2001), An introduction to statistical modeling of extremes values, *Springer*.

Dee, D.P. *et al.*, 2011. *The ERA-Interim reanalysis: configuration and performance of the data assimilation system. Royal Meteorological Society* Vol. 137, pp. 553-597.

Dias Pinto, J. R.; R. P. da Rocha. (2011), The energy cycle and structural evolution of cyclones over southeastern South America in three case studies. *Journal of Geophys*. Res.: Atmospheres, Vol. 116(D14).

DHN – Diretoria de Hidrografia e Navegação. Centro de Hidrografia da Marinha. Manual do Observador Meteorológico, disponível em: https://www.marinha.mil.br/chm/sites/www.m

arinha.mil.br.chm/files/u1907/manual-observador-completo.pdf , acesso em: 30 abr. 2020.

Embrechts, P.; Klüppelberg, C.; Mikosch, T. (1997), *Modelling Extremal Events*. Berlin, Heidelberg, Springer Berlin Heidelberg, (Stochastic Modelling and Applied Probability, v. 33), disponível em: <http://www.springerlink.com/index/10.1007/978-3-642-33483-2>

Fedorova, N. (1999), *Meteorologia sinótica,* Vol. 1, Pelotas, UFPEL.

Gan, M. A. (2009), Ciclone Catarina: análise sinótica, in *III SIMPÓSIO INTERNACIONAL DE CLIMATOLOGIA*, Canela - RS, 18 a 21 de outubro de 2009.

Godoi, V.A. (2011), Avaliação de Eventos Extremos de Ondas na Baía de Guanabara. Dissertação de Mestrado da COPPE/UFRJ, Rio de Janeiro.

Gomes, Tiago Francisco Pinheiro. (2018), *Eventos Extremos E Estruturas Coerentes Na Turbulência*: Estudo De Caso Para O Vento Solar.

Gozzo, L. F.; Rocha, R. P. da.; Reboita, M. S. e Sugahara, S. (2014), Subtropical Cyclones over the Southwestern South Atlantic: Climatological Aspects and Case Study. *J. Climate*, Vol. 27, pp. 8543–8562.

Hersbach, Hans *et al*. (2019). *Global reanalysis: goodbye ERA-Interim, hello ERA5*. European Centre for Medium-Range Weather Forecasts (ECMWF).

Holton, J. R. (1992), *An introduction to dynamic meteorology*. 3a ed, Elsevier Academic Press, New York.

Hosking, J. R. M.; Wallis, J. R. (1987). Parameter and quanMethods to calculate extreme wind speeds 131 tile estimation for the generalized Pareto distribution, *Technometrics*, Vol. 29, pp. 339–349.

Hoskins, B. J.; K. I. Hodges. (2005), A New Perspective on Southern Hemisphere Storm Tracks. *J. Climate*, Vol. 18, pp. 4108–4129.

Innocentini, V.; Caetano Neto, E. S. (1996)*, "*A case study of the 9 August 1998 South Atlantic storm: Numerical simulations of the wave activity*"*. *Wea. Forecasting*., Vol. 11, pp. 78-88.

Liska, G. R. *et al*. (2013a), Níveis de retorno de rajadas de vento via metodologias POT e blocos máximos no município de Piracicaba-SP. *Matemática e Estatística em Foco*, Vol. 1, No. 2.

Liska, G.R.; Bortolini, J.; Sáfadi, T.; Beijo, A. (2013b), Estimativas de velocidade máxima de vento em Piracicaba-SP via séries temporais e Teoria de Valores Extremos. *Revista Brasileira de Biometria*, Vol. 2, pp. 295-309.

Marengo, J.; Cornejo, A.; Satyamurty, P.; Nobre, C.A.; Sea, W. (1997), Cold surges in tropical and extratropical South America: The strong event in june 1994. *Monthly Weather Review*, Vol. 125, No.11, pp. 2759-2786.

Mazzaro, E.; Antonio, C.F.J.L.; Rangel, R.H.O.; Palmeira, R.M.J; Palmeira, A.C.P.A. (2019), Cenários Atmosféricos Precursores de Eventos de Ressaca Na Baia de Guanabara nos anos de 2017 e 2019 utilizando WRF. (Apresentação de Trabalho/Simpósio).

Melo Filho, E. (1993), *"The Sea Sentinels Project: Watching Waves in Brazil"*, in *Proceedings of 8th Symposium on Coastal and Ocean Management* (Coastal Zone), American Society of Civil Engineering, pp. 505-517.

OMM – Organização Meteorológica Mundial (OMM). (1997), *Manual on Codes:* International Codes. Vol. 1, Part A – Alphanumeric Codes. WMO - No. 306.

Oliveira, A. S. (1986), Interações entre sistemas frontais na América do Sul e convecção na Amazônia. (INPE-4008-TDL/239). Dissertação de Mestrado em Meteorologia do Instituto Nacional de Pesquisas Espaciais, São José dos Campos, 1986.

Oliveira, L.L.; Vianello, R.L.; Ferreira, N.J. (2001), Meteorologia Fundamental, Erichim, RS, EDIFAPES, 432 p.

PETROBRAS – Petróleo Brasileiro SA, disponível em: https://petrobras.com.br/pt/nossas-atividades/principais-operacoes/bacias/bacia-de-campos.htm, acesso em: 05 mar. 2020.

Parente, C. E. (1999), Uma Nova Técnica Espectral para Análise Direcional de Ondas. Tese de Doutorado da Universidade Federal do Rio de Janeiro.

Pinho, U. F. (2003), Caracterização dos estados de mar na Bacia de Campos. Tese de M.Sc., COPPE/UFRJ, Rio de Janeiro, RJ, Brasil.

Phillips, O. M. (1986), *The Dynamics of the Upper Ocean*. Cambridge University Press, 261 p.

Pond, S.; Pickard, G.L. (1983), *Introductory Dynamical Oceanography*, 2rid ed., 329 pp., Pergamon, New York.

Reboita, M. S. (2008), Ciclones Extratropicais sobre o Atlântico Sul: Simulação Climática e Experimentos de Sensibilidade. Tese de Doutorado em Meteorologia do Instituto de Astronomia, Geofísica e Ciências Atmosféricas – IAG–USP.

Saha, S.; Moorthi, S.; Pan, H. L.; Wu, X.; Wang, J.; Nadiga, S.; CK Tripp, P.; Kistler, R.; EN, J. W.; D Behringer, D.; LIU, H.; Stokes, D.; Grumbine, R.; Gayno, G.; Wang, J.; HOU, Y. T.; Chuang, H. Y.; Juang, H. M. H.; Sela, J.; Iredell, M.; Treadon, R.; Kleist, D.; T, P. V. D.; Keyser, D.; Derber, J.; EK, M.; E Meng, J.; Wei, H.; An Yang, R.; Lord, S.; Van Den Dool, H.; Kumar, A.; U Wang, W.; Long, C.; Iah, M. C.; Xue, Y.; N Huang, B.; Schemm, J. K.; EY Ebisuzaki, W.; Lin, R.; Xie, P.; Chen, M.; Zhou, S.; Higgins, W.; Zou, C. Z.; Liu, Q.; Chen, Y.; Han, Y.; Cucurull, L.; Reynolds, R. W.; Rutledge, G.; Goldberg, M. (2010). The NCEP climate forecast system reanalysis. *American Meteorological Society*, Vol. 91, pp. 1015–1057.

Sant'Anna, C. L. M. L. (2018), Estimativa de Quantis Extremos de vento como suporte ao dimensionamento de edificações, Monografia, Orientador: Otto Corrêa Rotunno Filho.

Silva, P. E. D. (2013). "Caracterização do padrão de ondas na costa do Brasil por meio de modelagem numérica". Dissertação de Mestrado. São José dos Campos, SP, Meteorologia, Instituto Nacional de Pesquisas Espaciais.

Silva, F.L.C. (2008), *Investigações sobre a chegada de ondulações (swell) em situações de bom tempo na Bacia de Campos*. Dissertação de Mestrado - COPPE/Universidade Federal do Rio de Janeiro, Rio de Janeiro, Brasil.

Silva, Natalia Pillar da. (2013), Extremos de vento sobre o Oeste do Oceano Atlântico Sul: análise direcional das ocorrências. Dissertação de Mestrado em Meteorologia do Instituto de Astronomia, Geofísica e Ciências Atmosféricas, Universidade de São Paulo, São Paulo, 2013, acesso em: 2020-07-16.

Simiu, E.; Heckert, N. A. (1996)*. Extreme wind distribution tails: a 'peaks-over-threshold' approach. *J. Struct. Eng.*, Vol. 122, pp. 539–547.

Sinclair, M. R. (1995), A climatology of cyclogenesis for the Southern Hemisphere. *Monthly Weather Review*, Vo. 123, pp. 1601-1619.

Zar, J. H. (1988), *Biostatistical Analysis*. 4. ed., United States of America, Prentice Hall, 916 p.